Rock and Soil Mechanics

Volume 42 | Issue 5 Article 5

9-16-2021

Dynamic response of a track coupled with a transversely isotropic ground due to train axle loads

Yi-cheng LI
Department of Geotechnical Engineering, Tongji University, Shanghai 200092, China

Shi-jin FENG
Key Laboratory of Geotechnical and Underground Engineering of the Ministry of Education, Tongji University, Shanghai 200092, China, fsjgly@tongji.edu.cn

Custom Citation

LI Yi-cheng, FENG Shi-jin, . Dynamic response of a track coupled with a transversely isotropic ground due to train axle loads[J]. Rock and Soil Mechanics, 2021, 42(5): 1313-1324.

Rock and Soil Mechanics 2021 42(5): 1313−1324 ISSN 1000−7598
https: //doi.org/10.16285/j.rsm.2020.6188 rocksoilmech.researchcommons.org/journal

Dynamic response of a track coupled with a transversely isotropic ground due to train axle loads

LI Yi-cheng[1], FENG Shi-jin[1, 2]

1. Department of Geotechnical Engineering, Tongji University, Shanghai 200092, China

2. Key Laboratory of Geotechnical and Underground Engineering of the Ministry of Education, Tongji University, Shanghai 200092, China

Abstract: To study the environmental vibrations induced by train loads, an analytical model for a track coupled with a layered transversely isotropic (TI) ground is developed. The model can consider the alternate distribution of TI elastic and poroelastic layers in the ground to describe soils and rocks under different moisture conditions compared with existing models comprising only one type of medium. Based on the analytical model, the governing equations of TI media are solved firstly using Fourier transform and a potential function method. Then the exact stiffness matrix method is adapted to derive solutions to the layered ground with different media. Finally, the dynamic response of the coupled system is obtained by using the governing equations of the track and inverse integral transformation. The influences of groundwater existence and transverse isotropy on the vibration of track and ground are investigated. It is found that the influence of the groundwater existence in the TI poroelastic layer on the track force amplification factor is significant at load frequency lower than 200 Hz. The ground surface vibration attenuates faster with the distance from the track center for a larger ratio of the horizontal elastic modulus to the vertical one. The maximum vertical stress magnitude occurs within 1 m from the ground surface. The critical speed of the displacement and stress increases with the increasing ratio of the horizontal elastic modulus to the vertical one.

Keywords: track; transversely isotropic; analytical model; alternate distribution; exact stiffness matrix; dynamic response

1 Introduction

Recently, the construction of high-speed railway boosts the development of economy and provides convenience to people. However, the increase of the train speed leads to more serious environmental vibrations[1], and this problem has a side effect on the train safety and the infrastructure around the railway. Thus, the dynamic response for coupled track–ground system has drawn widespread attention.

Analytical, numerical and experimental methods have been utilized to study the dynamic response for a track coupled with a ground, all of which the analytic method is widely used because of its high efficiency. For example, Dieterman et al.[2] solved the dynamic response problem of coupled beam–half space by simulating the track and the ground as the Euler beam and the half-space with homogeneous elastic medium, respectively, and introducing the equivalent dynamic stiffness. Sheng et al.[3] and Jones et al.[4] developed a more realistic analytical model for the track system. In this model, the ground was considered as a layered half-space ground with homogeneous elastic phase medium, and then the dynamic response of the track coupled a layered ground under the moving loads was analyzed. Feng et al.[5] analyzed the dynamic response of the track–elastic medium ground induced by a train under the condition of track irregularity. Huang et al.[6] compared the dynamic response of the Timoshenko beam with one-dimensional and three-dimensional elastic ground. The above study all considered the ground as a homogeneous or a layered elastic medium. For the groundwater, the Biot wave theory[7] of poroelastic medium was introduced. Jin[8] analyzed the dynamic response for the Euler beam with infinite length on the homogeneous saturated poroelastic medium. Xu et al.[9] analyzed the vibration problem of coupled system consisting of a layered saturated soil mass and the Euler beam, and solved the layered ground using TRM method. Cai et al.[10] investigated the vibrations of the trackhomogeneous saturated half-space coupled model under train loading. Cao et al.[11] studied the influence of the train loading induced by acceleration and speed reduction on the ground of the track on the saturated half-space. Ba et al.[1] discretized the interface of track foundation using IBEM, and analyzed the dynamic response of track system on layered saturated ground. Yao et al.[12] established a vibration prediction model of vehicle–rail– saturated half-space ground coupled system considering contact between the wheel and the rail.

In the aforementioned studies, the soil mass is regarded as an isotropic medium, but the ground is generally transversely isotropic due to the natural deposition of soil mass[13–15]. Thus, researchers investigated the dynamic response[22–25] of transversely isotropic(TI) elastic[16–21] or poroelastic medium under loading or vibration. Some researchers studied the vibration problem for a track coupled with the TI ground. Ba et al.[26] simulated the

Received: 10 August 2020 Revised: 6 January 2021
This work was supported by the National Science Fund for Distinguished Young Scholars (41725012).
First author: LI Yi-cheng, male, born in 1993, PhD candidate, majoring in soil dynamics and environmental vibration. E-mail: liyichengtj@foxmail.com
Corresponding author: FENG Shi-jin, male, born in 1978, PhD, Professor, PhD supervisor, mainly engaged in teaching and scientific research of soil dynamics and environmental geotechnical engineering. E-mail: fsjgly@tongji.edu.cn

ground as a layered TI elastic half-space and analyzed the genera- tion and propagation of dynamic response. Zhou et al.[27] researched the dynamic response of coupled system consisting of the track, the concrete layer and TI por- oelastic half-space. Zhan et al.[28] developed a model for the slab track coupled with layered TI saturated ground, and analyzed the influence of various parameters on vibration.

At present, the analytic research on the dynamic response for track–TI ground coupling system is limited, and in most of the previous studies, the ground was regarded as one medium (the elastic or poroelastic saturated medium). However, in practice, various strata have different saturated conditions. Thus, these strata could be regarded as various TI mediums. Recently, Li et al.[29] developed a ground model with alternate TI elastic medium and poroelastic medium. In this model, TI elastic medium, TI poroelastic medium and TI elastic half-space were used to simulated the soil layers above the groundwater table, saturated soil layers and the bottom layer such as bedrock. However, Li et al.[29] just analyzed the dynamic response of ground model induced by moving source, but the vibration propagation of the coupling system caused by the train loading was not investigated. In addition, Li et al.[29] just gave the solution for the 3-layer ground model.

Based on the previous studies, this paper establishes an analytical model of coupled track multi-layer ground considering the alternate distribution of TI elastic, poroelastic and elastic mediums. Compared with the existing track–elastic medium ground coupling model, this model can simulate TI layers with different water contents, taking into account the influences of groundwater and underlying layer. In order to solve the model, Fourier transform and potential function method are used to solve the dynamic equations of TI poroelastic and elastic media, respectively. Then, the exact stiffness matrix method is adapted to derive solutions of layered ground with arbitrary layers and different TI mediums. By combining the track control equation, the analytical solution of the dynamic response of the track–ground coupling system in the transformation domain is derived. Finally, the inverse Fourier transform is used to obtain the response in the space–time domain.

2 Mechanical model and the solution of governing equation

The model used in this paper is shown in Fig. 1. The track system consists of rail, rail pad, sleeper and ballast, and the ground model consists of three TI layers. In the ground model, the three TI layers include N_1 TI elastic medium layers, N_2 TI poroelastic medium layers and N_3 TI elastic medium layers, respectively, and the TI elastic half-space is at the bottom of the model. These three layers are utilized to simulate the TI layer above the groundwater table, the TI saturated layer and the underlying TI layer. The z coordinate of the lower boundary of i-th layer is z_i (i = 1, 2,…, N_1+N_2+N_3), the thickness of $h_i = z_i - z_{i-1}$.

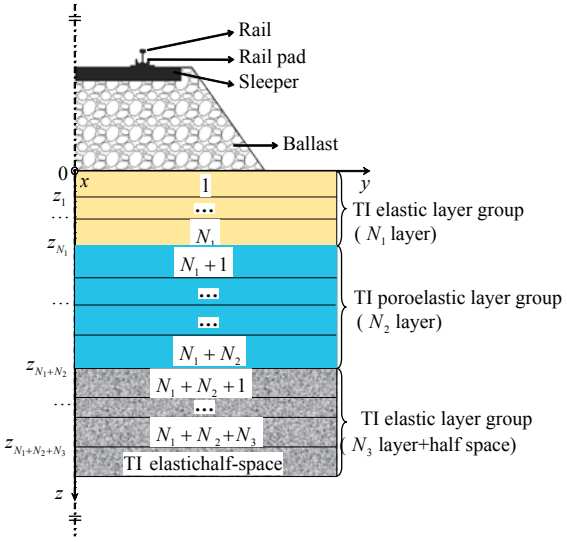

Fig. 1 Schematic diagram of model

2.1 Governing equations and solutions

The dynamic governing equations of poroelastic transversely isotropic (TI) medium in the coordinate are as follows[23]:

$$\sigma_{ij,j} = \rho\ddot{u}_i + \rho_f\ddot{w}_i \tag{1}$$

$$-p_{,i} = \rho_f\ddot{u}_i + r_l\dot{w}_i + m_l\ddot{w}_i \tag{2}$$

$$\frac{1}{M}p = -\alpha_1\frac{\partial u_x}{\partial x} - \alpha_1\frac{\partial u_y}{\partial y} - \alpha_3\frac{\partial u_z}{\partial z} - \frac{\partial w_x}{\partial x} - \frac{\partial w_y}{\partial y} - \frac{\partial w_z}{\partial z} \tag{3}$$

$$\left.\begin{aligned}
\sigma_{xx} &= c_{11}\frac{\partial u_x}{\partial x} + c_{12}\frac{\partial u_y}{\partial y} + c_{13}\frac{\partial u_z}{\partial z} - \alpha_1 p \\
\sigma_{yz} &= c_{44}\left(\frac{\partial u_y}{\partial z} + \frac{\partial u_z}{\partial y}\right) \\
\sigma_{yy} &= c_{12}\frac{\partial u_x}{\partial x} + c_{11}\frac{\partial u_y}{\partial y} + c_{13}\frac{\partial u_z}{\partial z} - \alpha_1 p \\
\sigma_{zx} &= c_{44}\left(\frac{\partial u_x}{\partial z} + \frac{\partial u_z}{\partial x}\right) \\
\sigma_{zz} &= c_{13}\frac{\partial u_x}{\partial x} + c_{13}\frac{\partial u_y}{\partial y} + c_{33}\frac{\partial u_z}{\partial z} - \alpha_3 p \\
\sigma_{xy} &= c_{66}\left(\frac{\partial u_x}{\partial y} + \frac{\partial u_y}{\partial x}\right)
\end{aligned}\right\} \tag{4}$$

$$\alpha_1 = 1 - \frac{2c_{11} - 2c_{66} + c_{13}}{3K_s},\ \alpha_3 = 1 - \frac{2c_{13} + c_{33}}{3K_s} \tag{5}$$

$$\frac{1}{M} = \frac{1}{K_s}\left(\frac{2\alpha_1 + \alpha_3}{3} - n\right) + \frac{n}{K_f} \tag{6}$$

where $\sigma_{ij}(i, j = x, y, z)$ and p are the stress tensor and the excess pore pressure, respectively; u_i is the displacement of soil skeleton; $w_i = n(U_i - u_i)$ represents the relative displacement between fluid and solid; U_i and n are the fluid displacement and the soil porosity, respectively; $\rho = (1-n)\rho_s + n\rho_f$ is the equivalent

density, and ρ_{s}, ρ_{f} are the skeleton and the fluid density, respectively; $r_l=\eta_{\mathrm{f}}/k_l$, and η_{f}, k_l are the dynamic viscosity of pore fluid and the inherent permeability coefficient of soil; $m_l=\alpha_{\infty l}\rho_{\mathrm{f}}/n$, and $\alpha_{\infty l}$ is the bending coefficient of porous medium. In the subscript of above symbols, $l=1$，3 corresponds to the horizontal and vertical variables, respectively. α_1, α_3 and M are the Biot parameters; K_{s} and K_{f} are the bulk modulii of soil skeleton and fluid, respectively; and c_{11}, c_{12}, c_{13}, c_{33}, c_{44} and c_{66} are the elastic parameters. It should be noted that, in the engineering, the elastic modulus (E_{h}, E_{v} corresponding to the horizontal and vertical), the shear modulus (G_{v}) and the Poisson's ratio (ν_{h}, ν_{vh} corresponding to the horizontal Poisson's ratio and the Poisson's ratio descripting the horizontal strain caused by the vertical stress) are typicaly used to describe the transversely isotropic medium, so these concepts were introduced into this paper. The relationship between elastic parameters and engineering parameters could be found in the reference [17].

The definitions of Fourier transform about *x*, *y* and *t* are as follows:

$$\left.\begin{aligned}&\overline{f}(\omega)=\int_{-\infty}^{\infty}f(t)\mathrm{e}^{-\mathrm{i}\omega t}\mathrm{d}t,\ f(t)=\frac{1}{2\pi}\int_{-\infty}^{\infty}\overline{f}(\omega)\mathrm{e}^{\mathrm{i}\omega t}\mathrm{d}\omega\\&\hat{f}(\xi)=\int_{-\infty}^{\infty}f(x)\mathrm{e}^{\mathrm{i}\xi x}\mathrm{d}x,\ f(x)=\frac{1}{2\pi}\int_{-\infty}^{\infty}\hat{f}(\xi)\mathrm{e}^{-\mathrm{i}\xi x}\mathrm{d}\xi\\&\tilde{f}(\eta)=\int_{-\infty}^{\infty}f(y)\mathrm{e}^{\mathrm{i}\eta y}\mathrm{d}y,\ f(y)=\frac{1}{2\pi}\int_{-\infty}^{\infty}\tilde{f}(\eta)\mathrm{e}^{-\mathrm{i}\eta y}\mathrm{d}\eta\end{aligned}\right\}\quad(7)$$

where ω is the circular frequency; ξ and η are the wave numbers corresponding to *x* and *y* directions, respectively; and i is the imaginary unit, $\mathrm{i}=\sqrt{-1}$.

Second-order linear differential equations of *u*-*p* form in frequency domain could be obtained after Fourier transforming Eqs. (1)–(4) with respect to *t* and arranging the results. These equations were solved using the potential function method[16]. Based on the method, the displacement and the excess pore pressure are as follows after introducing two potential functions *g* and φ:

$$\overline{u}_x=\frac{\partial^2}{\partial x\partial z}\left[a_2a_3-a_1\left(\beta_1\nabla_{\mathrm{d}}^2-\frac{1}{M}+\beta_3\frac{\partial^2}{\partial z^2}\right)\right]g-\frac{\partial\varphi}{\partial y}\quad(8)$$

$$\overline{u}_y=\frac{\partial^2}{\partial y\partial z}\left[a_2a_3-a_1\left(\beta_1\nabla_{\mathrm{d}}^2-\frac{1}{M}+\beta_3\frac{\partial^2}{\partial z^2}\right)\right]g+\frac{\partial\varphi}{\partial x}\quad(9)$$

$$\overline{u}_z=\left[\left(\beta_1\nabla_{\mathrm{d}}^2-\frac{1}{M}+\beta_3\frac{\partial^2}{\partial z^2}\right)\cdot\left(\rho_l^*\omega^2+c_{11}\nabla_{\mathrm{d}}^2+c_{44}\frac{\partial^2}{\partial z^2}\right)-a_2^2\nabla_{\mathrm{d}}^2\right]g\quad(10)$$

$$\overline{p}=\frac{\partial}{\partial z}\left[a_3\left(\rho_l^*\omega^2+c_{11}\nabla_{\mathrm{d}}^2+c_{44}\frac{\partial^2}{\partial z^2}\right)-a_1a_2\nabla_{\mathrm{d}}^2\right]g\quad(11)$$

where $\overline{u}_x$, $\overline{u}_y$ and $\overline{u}_z$ are the displacements in the three different directions in frequency domain; $\overline{p}$ is the pore pressure in the frequency domain; a_1, a_2, a_3, ρ_l^*, β_1 and β_3 are the intermediate variables; $\nabla_{\mathrm{d}}^2=\partial^2/\partial x^2+\partial^2/\partial y^2$; and

$$\beta_l=1/\left(\mathrm{i}\omega r_l-m_l\omega^2\right),\ l=1,3\quad(12)$$

$$\rho_l^*=\rho+\beta_l\rho_{\mathrm{f}}^2\omega^2,\ l=1,3\quad(13)$$

$$a_1=c_{13}+c_{44},\ a_2=\alpha_1+\beta_1\rho_{\mathrm{f}}\omega^2,\ a_3=\alpha_3+\beta_3\rho_{\mathrm{f}}\omega^2\quad(14)$$

By substituting Eqs. (8)–(11) into Eqs. (1)–(4) and combining with Fourier transform, the analytical solution to the dynamic equation of TI poroelastic medium in frequency domain-wavenumber domain could be derived, and the element stiffness matrix of the relationship between the displacements and stresses of the upper and lower boundary could be further established for arbitrary TI poroelastic layer:

$$\underbrace{\begin{bmatrix}\boldsymbol{S}_{\mathrm{p}}^{\mathrm{D}}&\boldsymbol{S}_{\mathrm{p}}^{\mathrm{U}}\boldsymbol{Z}_{\mathrm{p}}^{\mathrm{D}}\\-\boldsymbol{S}_{\mathrm{p}}^{\mathrm{D}}\boldsymbol{Z}_{\mathrm{p}}^{\mathrm{D}}&-\boldsymbol{S}_{\mathrm{p}}^{\mathrm{U}}\end{bmatrix}\begin{bmatrix}\boldsymbol{D}_{\mathrm{p}}^{\mathrm{D}}&\boldsymbol{D}_{\mathrm{p}}^{\mathrm{U}}\boldsymbol{Z}_{\mathrm{p}}^{\mathrm{D}}\\\boldsymbol{D}_{\mathrm{p}}^{\mathrm{D}}\boldsymbol{Z}_{\mathrm{p}}^{\mathrm{D}}&\boldsymbol{D}_{\mathrm{p}}^{\mathrm{U}}\end{bmatrix}^{-1}}_{\boldsymbol{K}_{\mathrm{p}}^{(n)}(\xi,\eta,h_n,\omega)}\begin{Bmatrix}\hat{\tilde{\boldsymbol{u}}}_{\mathrm{p}}(z_{n-1}^+)\\\hat{\tilde{\boldsymbol{u}}}_{\mathrm{p}}(z_n^-)\end{Bmatrix}=\begin{Bmatrix}\hat{\tilde{\boldsymbol{\Sigma}}}_{\mathrm{p}}(z_{n-1}^+)\\-\hat{\tilde{\boldsymbol{\Sigma}}}_{\mathrm{p}}(z_n^-)\end{Bmatrix}\quad(15)$$

where $\boldsymbol{S}_{\mathrm{p}}^{\mathrm{D}}$ and $\boldsymbol{S}_{\mathrm{p}}^{\mathrm{U}}$ are stress-dependent submatrix, D and U in the superscript represent the submatrix corresponding to the downgoing and the upgoing waves, and p in the subscript represents the matrix corresponding to TI poroelastic medium; $\boldsymbol{D}_{\mathrm{p}}^{\mathrm{D}}$ and $\boldsymbol{D}_{\mathrm{p}}^{\mathrm{U}}$ are the displacement-related submatrix; $\boldsymbol{Z}_{\mathrm{p}}^{\mathrm{D}}$ is the diagonal matrix of exponential term; h_n is the thickness of *n*-th layer; $\hat{\tilde{\boldsymbol{u}}}_{\mathrm{p}}$ is the displacement vector and $\hat{\tilde{\boldsymbol{\Sigma}}}_{\mathrm{p}}$ is the stress vector. z_n^- and z_{n-1}^+ denote the upward side of the boundary $z=z_n$ and the downward side of the boundary $z=z_{n-1}$. The definitions of above symbols are as follows:

$$\hat{\tilde{\boldsymbol{u}}}_{\mathrm{p}}(z_n^{\pm})=\left[\hat{\tilde{u}}_x^{\mathrm{p}}(z_n^{\pm}),\hat{\tilde{u}}_y^{\mathrm{p}}(z_n^{\pm}),\hat{\tilde{u}}_z^{\mathrm{p}}(z_n^{\pm}),\hat{\tilde{w}}_z^{\mathrm{p}}(z_n^{\pm})\right]^{\mathrm{T}}\quad(16)$$

$$\hat{\tilde{\boldsymbol{\Sigma}}}_{\mathrm{p}}(z_n^{\pm})=\left[\hat{\tilde{\sigma}}_{xz}^{\mathrm{p}}(z_n^{\pm}),\hat{\tilde{\sigma}}_{yz}^{\mathrm{p}}(z_n^{\pm}),\hat{\tilde{\sigma}}_{zz}^{\mathrm{p}}(z_n^{\pm}),\hat{\tilde{p}}^{\mathrm{p}}(z_n^{\pm})\right]^{\mathrm{T}}\quad(17)$$

$$\boldsymbol{Z}_{\mathrm{p}}^{\mathrm{D}}\left(h_n\right)=\mathrm{diag}\left[\mathrm{e}^{-\lambda_1h_n},\mathrm{e}^{-\lambda_2h_n},\mathrm{e}^{-\lambda_3h_n},\mathrm{e}^{-\lambda_4h_n}\right]\quad(18)$$

where $\hat{\tilde{w}}_z^{\mathrm{p}}$ is the relative displacement between solid and fluid in *z* direction; $\hat{\tilde{\sigma}}_{xz}^{\mathrm{p}}$, $\hat{\tilde{\sigma}}_{yz}^{\mathrm{p}}$ and $\hat{\tilde{\sigma}}_{zz}^{\mathrm{p}}$ are the stresses of poroelastic medium; $\hat{\tilde{p}}^{\mathrm{p}}$ is the pore pressure of poroelastic medium; the symbols over the variables represent the variables in frequency–wave number domain.

The relevant elements of the displacement–stress matrix are defined as follows. D_{1i}^{Dp} represents the element in the 1st row and the *i*-th column of $\boldsymbol{D}_{\mathrm{p}}^{\mathrm{D}}$, and other symbols are defined similarly.

$$\left.\begin{aligned}
&D_{1i}^{Dp}=-D_{1i}^{Up}=\mathrm{i}\xi\chi_i\ (i=1,2,3),\ D_{14}^{Dp}=D_{14}^{Up}=\eta\\
&D_{2i}^{Dp}=-D_{2i}^{Up}=\mathrm{i}\eta\chi_i\ (i=1,2,3),\ D_{24}^{Dp}=D_{24}^{Up}=-\xi\\
&D_{3i}^{Dp}=D_{3i}^{Up}=\gamma_i\ (i=1,2,3),\ D_{34}^{Dp}=D_{34}^{Up}=0\\
&D_{4i}^{Dp}=D_{4i}^{Up}=\beta_3\left(\rho_{\mathrm{f}}\omega^2\gamma_i-\kappa_i\lambda_i\right)(i=1,2,3),\\
&D_{44}^{Dp}=D_{44}^{Up}=0
\end{aligned}\right\}\tag{19}$$

where λ_i, γ_i and χ_i are the intermediate variables.

$$\left.\begin{aligned}
&S_{1i}^{Dp}=S_{1i}^{Up}=-\mathrm{i}\xi c_{44}\left(\chi_i\lambda_i+\gamma_i\right)(i=1,2,3),\\
&S_{14}^{Dp}=-S_{14}^{Up}=-\eta c_{44}\lambda_4\\
&S_{2i}^{Dp}=S_{2i}^{Up}=-\mathrm{i}\eta c_{44}\left(\chi_i\lambda_i+\gamma_i\right)(i=1,2,3),\\
&S_{24}^{Dp}=-S_{24}^{Up}=\xi c_{44}\lambda_4\\
&S_{3i}^{Dp}=-S_{3i}^{Up}=\vartheta_i\ (i=1,2,3),\ S_{34}^{Dp}=S_{34}^{Up}=0\\
&S_{4i}^{Dp}=-S_{4i}^{Up}=-\kappa_i\ (i=1,2,3),\ S_{44}^{Dp}=S_{44}^{Up}=0
\end{aligned}\right\}\tag{20}$$

where κ_i and ϑ_i are the intermediate variables.

$\pm\lambda_i$ ($i=1,2,3$) are the eigenvalues of the following six order ordinary differential equation:

$$\left(b_1\frac{\partial^6}{\partial z^6}+b_2\frac{\partial^4}{\partial z^4}+b_3\frac{\partial^2}{\partial z^2}+b_4\right)g=0\tag{21}$$

$$\lambda_4=\sqrt{\left[c_{66}(\xi^2+\eta^2)-\rho_1^*\omega^2\right]/c_{44}}\tag{22}$$

The other symbols in Eqs. (19)–(20) are defined as follow[29]:

$$\gamma_i=\left(a_4+c_{44}\lambda_i^2\right)\left(a_6+\beta_3\lambda_i^2\right)+a_2^2\left(\xi^2+\eta^2\right),i=1,2,3\tag{23}$$

$$\chi_i=\lambda_i\left[a_2a_3-a_1\left(a_6+\beta_3\lambda_i^2\right)\right],i=1,2,3\tag{24}$$

$$\kappa_i=\left[a_3\left(a_4+c_{44}\lambda_i^2\right)+a_1a_2\left(\xi^2+\eta^2\right)\right]\lambda_i,i=1,2,3\tag{25}$$

$$\vartheta_i=c_{13}\left(\xi^2+\eta^2\right)\chi_i+\alpha_3\kappa_i-c_{33}\lambda_i\gamma_i,\quad i=1,2,3\tag{26}$$

$$\left.\begin{aligned}
&a_4=\rho_1^*\omega^2-c_{11}\left(\xi^2+\eta^2\right),a_5=\rho_3^*\omega^2-c_{44}\left(\xi^2+\eta^2\right)\\
&a_6=-\frac{1}{M}-\beta_1\left(\xi^2+\eta^2\right)
\end{aligned}\right\}\tag{27}$$

$$\left.\begin{aligned}
&b_1=c_{33}c_{44}\beta_3\\
&b_2=c_{33}c_{44}a_6+c_{44}\beta_3a_5+c_{33}\beta_3a_4+a_1^2\beta_3(\xi^2+\eta^2)-a_3^2c_{44}\\
&b_3=a_4a_5\beta_3+c_{44}a_5a_6+c_{33}a_4a_6-2a_1a_2a_3\left(\xi^2+\eta^2\right)+\\
&\quad a_2^2c_{33}\left(\xi^2+\eta^2\right)+a_1^2a_6\left(\xi^2+\eta^2\right)-a_3^2a_4\\
&b_4=a_4a_5a_6+a_2^2a_5\left(\xi^2+\eta^2\right)
\end{aligned}\right\}\tag{28}$$

The above is the general solution of TI poroelastic medium, and the dynamic governing equation of TI elastic medium is as follows[20]:

$$\sigma_{ij,j}^{\mathrm{e}}=\rho^{\mathrm{e}}\ddot{u}_i^{\mathrm{e}}\tag{29}$$

where ρ^{e} is the density of elastic medium; $\ddot{u}_i^{\mathrm{e}}$ is the second partial derivative of displacement with respect to time; $\sigma_{ij,j}^{\mathrm{e}}$ is the first partial derivative of stress with respect to spatial coordinates. In addition,

$$\left.\begin{aligned}
&\sigma_{xx}^{\mathrm{e}}=c_{11}^{\mathrm{e}}\frac{\partial u_x^{\mathrm{e}}}{\partial x}+c_{12}^{e}\frac{\partial u_y^{\mathrm{e}}}{\partial y}+c_{13}^{\mathrm{e}}\frac{\partial u_z^{\mathrm{e}}}{\partial z},\sigma_{yz}^{\mathrm{e}}=c_{44}^{\mathrm{e}}\left(\frac{\partial u_y^{\mathrm{e}}}{\partial z}+\frac{\partial u_z^{\mathrm{e}}}{\partial y}\right)\\
&\sigma_{yy}^{\mathrm{e}}=c_{12}^{\mathrm{e}}\frac{\partial u_x^{\mathrm{e}}}{\partial x}+c_{11}^{\mathrm{e}}\frac{\partial u_y^{\mathrm{e}}}{\partial y}+c_{13}^{\mathrm{e}}\frac{\partial u_z^{\mathrm{e}}}{\partial z},\sigma_{zx}^{\mathrm{e}}=c_{44}^{\mathrm{e}}\left(\frac{\partial u_x^{\mathrm{e}}}{\partial z}+\frac{\partial u_z^{\mathrm{e}}}{\partial x}\right)\\
&\sigma_{zz}^{\mathrm{e}}=c_{13}^{\mathrm{e}}\frac{\partial u_x^{\mathrm{e}}}{\partial x}+c_{13}^{\mathrm{e}}\frac{\partial u_y^{\mathrm{e}}}{\partial y}+c_{33}^{\mathrm{e}}\frac{\partial u_z^{\mathrm{e}}}{\partial z},\sigma_{xy}^{\mathrm{e}}=c_{66}^{\mathrm{e}}\left(\frac{\partial u_x^{\mathrm{e}}}{\partial y}+\frac{\partial u_y^{\mathrm{e}}}{\partial x}\right)
\end{aligned}\right\}\tag{30}$$

The element stiffness matrices of TI elastic layer and half-space are shown as follow:

$$\underbrace{\begin{bmatrix}\boldsymbol{S}_{\mathrm{e}}^{\mathrm{D}} & \boldsymbol{S}_{\mathrm{e}}^{\mathrm{U}}\boldsymbol{Z}_{\mathrm{e}}^{\mathrm{D}}\\ -\boldsymbol{S}_{\mathrm{e}}^{\mathrm{D}}\boldsymbol{Z}_{\mathrm{e}}^{\mathrm{D}} & -\boldsymbol{S}_{\mathrm{e}}^{\mathrm{U}}\end{bmatrix}\begin{bmatrix}\boldsymbol{D}_{\mathrm{e}}^{\mathrm{D}} & \boldsymbol{D}_{\mathrm{e}}^{\mathrm{U}}\boldsymbol{Z}_{\mathrm{e}}^{\mathrm{D}}\\ \boldsymbol{D}_{\mathrm{e}}^{\mathrm{D}}\boldsymbol{Z}_{\mathrm{e}}^{\mathrm{D}} & \boldsymbol{D}_{\mathrm{e}}^{\mathrm{U}}\end{bmatrix}^{-1}}_{\boldsymbol{K}_{\mathrm{e}}^{(n)}(\xi,\eta,h_n,\omega)}\begin{Bmatrix}\hat{\hat{\boldsymbol{u}}}_{\mathrm{e}}(z_{n-1}^+)\\ \hat{\hat{\boldsymbol{u}}}_{\mathrm{e}}(z_n^-)\end{Bmatrix}=\begin{Bmatrix}\hat{\hat{\boldsymbol{\Sigma}}}_{\mathrm{e}}(z_{n-1}^+)\\ -\hat{\hat{\boldsymbol{\Sigma}}}_{\mathrm{e}}(z_n^-)\end{Bmatrix}\tag{31}$$

$$\underbrace{\left[\boldsymbol{S}_{\mathrm{e}}^{\mathrm{D}}\right]\left[\boldsymbol{D}_{\mathrm{e}}^{\mathrm{D}}\right]^{-1}}_{\boldsymbol{K}_{\mathrm{e}}^{\text{half-space}}}\left\{\hat{\hat{\boldsymbol{u}}}_{\mathrm{e}}(z_n^+)\right\}=\left\{\hat{\hat{\boldsymbol{\Sigma}}}_{\mathrm{e}}(z_n^+)\right\}\tag{32}$$

where $\boldsymbol{S}_{\mathrm{e}}^{\mathrm{D}}$, $\boldsymbol{S}_{\mathrm{e}}^{\mathrm{U}}$ are stress-related submatrices, in which the definitions of superscript are similar to those in Eq. (15), and the subscript "e" represents TI elastic medium related matrix; $\boldsymbol{D}_{\mathrm{e}}^{\mathrm{D}}$ and $\boldsymbol{D}_{\mathrm{e}}^{\mathrm{U}}$ are the displacement-related submatrices; $\boldsymbol{Z}_{\mathrm{e}}^{\mathrm{D}}$ is the exponential diagonal matrix; $\hat{\hat{\boldsymbol{u}}}_{\mathrm{e}}$ and $\hat{\hat{\boldsymbol{\Sigma}}}_{\mathrm{e}}$ are the displacement and stress vectors, respectively; and $\boldsymbol{K}_{\mathrm{e}}^{\text{half-space}}$ is the stiffness matrix of half-space.

2.2 Dynamic response of layered half space incorporating different TI mediums

After acquiring the element stiffness matrices in Eqs. (15), (31) and (32), the dynamic response of layered ground is solved based on the exact stiffness matrix method[30]. In this model, the alternating layers of elastic and poroelastic TI mediums are considered. It is noted that the displacement and stress vectors at the interface between the two medium layers contain 3 and 4 control variables, respectively (the elastic medium layer does not contain fluid-related control variables), and the dimensions of corresponding element stiffness matrices are 6×6 and 8×8, respectively. The difference in dimensions of them has a side effect on the assembly of the total stiffness matrix and the solution of the problem. Therefore, the classical exact stiffness matrix method is extended in this section. The element stiffness matrix of TI poroelastic medium layer is preprocessed, and the number of control variables at the interface between different medium layers can be equal. And it is convenient to directly assemble and inverse the total stiffness matrix.

In the model shown in Fig.1, the boundaries at $z=z_{N_1+1}$ and $z=z_{N_1+N_2}$ are the interfaces between the different mediums. The interface at $z=z_{N_1+N_2}$ is taken as an example for solving.

Based on Eq. (15), the element stiffness matrix for layer N_1+N_2 TI poroelastic medium could be described as

$$\boldsymbol{K}_{\mathrm{p}}^{(N_1+N_2)}\begin{Bmatrix}\hat{\hat{\boldsymbol{u}}}_{\mathrm{p}}(z^{+}_{N_1+N_2-1})\\ \hat{\hat{u}}^{\mathrm{p}}_{x}(z^{-}_{N_1+N_2})\\ \hat{\hat{u}}^{\mathrm{p}}_{y}(z^{-}_{N_1+N_2})\\ \hat{\hat{u}}^{\mathrm{p}}_{z}(z^{-}_{N_1+N_2})\\ \hat{\hat{w}}^{\mathrm{p}}_{z}(z^{-}_{N_1+N_2})\end{Bmatrix}=\begin{Bmatrix}\hat{\hat{\boldsymbol{\Sigma}}}_{\mathrm{p}}(z^{+}_{N_1+N_2-1})\\ -\hat{\hat{\sigma}}^{\mathrm{p}}_{xz}(z^{-}_{N_1+N_2})\\ -\hat{\hat{\sigma}}^{\mathrm{p}}_{yz}(z^{-}_{N_1+N_2})\\ -\hat{\hat{\sigma}}^{\mathrm{p}}_{zz}(z^{-}_{N_1+N_2})\\ -\hat{\hat{p}}^{\mathrm{p}}(z^{-}_{N_1+N_2})\end{Bmatrix} \tag{33}$$

The variables with subscripts, "–" and "+", represent the control variables above and below the interface, respectively. $\hat{\hat{\boldsymbol{u}}}_{\mathrm{p}}(z^{+}_{N_1+N_2-1})$ and $\hat{\hat{\boldsymbol{\Sigma}}}_{\mathrm{p}}(z^{+}_{N_1+N_2-1})$ are the displacement and stress vectors of the upper boundary of the layer N_1+ N_2, and each vector includes four control variables. Detail information for the vectors of the upper boundary is not needed because it is not necessary to dispose, and the equations about them are similar to Eqs. (16) and (17). $\hat{\hat{u}}^{\mathrm{p}}_{x}(z^{-}_{N_1+N_2})$ and $\hat{\hat{u}}^{\mathrm{p}}_{x}(z^{-}_{N_1+N_2})$ are the displacement and the stress control variables of the lower boundary of layer N_1 + N_2. $\boldsymbol{K}_{\mathrm{p}}^{(N_1+N_2)}$ is a stiffness matrix with 8×8.

Firstly, 8-th line in Eq. (33) is extracted for eliminating the pore pressure variable $\hat{\hat{p}}^{\mathrm{p}}(z^{-}_{N_1+N_2})$, and the following equation could be obtained:

$$\boldsymbol{K}_{\mathrm{p}}^{(N_1+N_2)}(1\sim 7,1\sim 8)\begin{Bmatrix}\hat{\hat{\boldsymbol{u}}}_{\mathrm{p}}(z^{+}_{N_1+N_2-1})\\ \hat{\hat{u}}^{\mathrm{p}}_{x}(z^{-}_{N_1+N_2})\\ \hat{\hat{u}}^{\mathrm{p}}_{y}(z^{-}_{N_1+N_2})\\ \hat{\hat{u}}^{\mathrm{p}}_{z}(z^{-}_{N_1+N_2})\\ \hat{\hat{w}}^{\mathrm{p}}_{z}(z^{-}_{N_1+N_2})\end{Bmatrix}=\begin{Bmatrix}\hat{\hat{\boldsymbol{\Sigma}}}_{\mathrm{p}}(z^{+}_{N_1+N_2-1})\\ -\hat{\hat{\sigma}}^{\mathrm{p}}_{xz}(z^{-}_{N_1+N_2})\\ -\hat{\hat{\sigma}}^{\mathrm{p}}_{yz}(z^{-}_{N_1+N_2})\\ -\hat{\hat{\sigma}}^{\mathrm{p}}_{zz}(z^{-}_{N_1+N_2})\end{Bmatrix} \tag{34}$$

where $\boldsymbol{K}_{\mathrm{p}}^{(N_1+N_2)}$(1–7, 1–8) represents the elements in rows 1–7 and columns 1–8 of the matrix $\boldsymbol{K}_{\mathrm{p}}^{(N_1+N_2)}$, and other similar symbols have similar definitions.

Then, the variable of vertical relative displacement of fluid $\hat{\hat{w}}^{\mathrm{p}}_{z}(z^{-}_{N_1+N_2})$ is eliminated. The selection of elimination method depends on the drainage conditions at the lower boundary $z=z_{N_1+N_2}$.

If the lower boundary is a drainage boundary, $\hat{\hat{p}}^{\mathrm{p}}(z^{-}_{N_1+N_2})=0$ and the 8-th row in Eq. (33) is given as follows:

$$\hat{\hat{w}}^{\mathrm{p}}_{z}(z^{-}_{N_1+N_2})=-\frac{\boldsymbol{K}_{\mathrm{p}}^{(N_1+N_2)}(8,1\sim 7)}{\boldsymbol{K}_{\mathrm{p}}^{(N_1+N_2)}(8,8)}\begin{Bmatrix}\hat{\hat{\boldsymbol{u}}}_{\mathrm{p}}(z^{+}_{N_1+N_2-1})\\ \hat{\hat{u}}^{\mathrm{p}}_{x}(z^{-}_{N_1+N_2})\\ \hat{\hat{u}}^{\mathrm{p}}_{y}(z^{-}_{N_1+N_2})\\ \hat{\hat{u}}^{\mathrm{p}}_{z}(z^{-}_{N_1+N_2})\end{Bmatrix} \tag{35}$$

Substituting Eq.(35) into Eq.(34), the adapted element stiffness matrix of layer N_1+N_2 could be obtained when the lower boundary is the drainage condition.

$$\boldsymbol{K}_{\text{p-ad-p}}^{(N_1+N_2)}\begin{Bmatrix}\hat{\hat{\boldsymbol{u}}}_{\mathrm{p}}(z^{+}_{N_1+N_2-1})\\ \hat{\hat{u}}^{\mathrm{p}}_{x}(z^{-}_{N_1+N_2})\\ \hat{\hat{u}}^{\mathrm{p}}_{y}(z^{-}_{N_1+N_2})\\ \hat{\hat{u}}^{\mathrm{p}}_{z}(z^{-}_{N_1+N_2})\end{Bmatrix}=\begin{Bmatrix}\hat{\hat{\boldsymbol{\Sigma}}}_{\mathrm{p}}(z^{+}_{N_1+N_2-1})\\ -\hat{\hat{\sigma}}^{\mathrm{p}}_{xz}(z^{-}_{N_1+N_2})\\ -\hat{\hat{\sigma}}^{\mathrm{p}}_{yz}(z^{-}_{N_1+N_2})\\ -\hat{\hat{\sigma}}^{\mathrm{p}}_{zz}(z^{-}_{N_1+N_2})\end{Bmatrix} \tag{36}$$

where "ad" in the subscript means the adapted stiffness matrix, and "p" after "ad" means the drainage boundary. And

$$\boldsymbol{K}_{\text{p-ad-p}}^{(N_1+N_2)}(i,j)=\boldsymbol{K}_{\mathrm{p}}^{(N_1+N_2)}(i,j)-\frac{\boldsymbol{K}_{\mathrm{p}}^{(N_1+N_2)}(i,8)\times\boldsymbol{K}_{\mathrm{p}}^{(N_1+N_2)}(8,j)}{\boldsymbol{K}_{\mathrm{p}}^{(N_1+N_2)}(8,8)},1\leqslant i,j\leqslant 7 \tag{37}$$

If the lower boundary is impermeable boundary, $\hat{\hat{w}}^{\mathrm{p}}_{z}(z^{-}_{\mathrm{N_1+N_2}})=0$ and the 8-th row in Eq. (33) is shown as follows:

$$\hat{\hat{p}}^{\mathrm{p}}(z^{-}_{N_1+N_2})=-\boldsymbol{K}_{\mathrm{p}}^{(N_1+N_2)}(8,1\sim 7)\begin{Bmatrix}\hat{\hat{\boldsymbol{u}}}_{\mathrm{p}}(z^{+}_{N_1+N_2-1})\\ \hat{\hat{u}}^{\mathrm{p}}_{x}(z^{-}_{N_1+N_2})\\ \hat{\hat{u}}^{\mathrm{p}}_{y}(z^{-}_{N_1+N_2})\\ \hat{\hat{u}}^{\mathrm{p}}_{z}(z^{-}_{N_1+N_2})\end{Bmatrix} \tag{38}$$

Substituting the impermeable boundary condition into Eq. (34), the similar equation with Eq. (36) could be obtained. The difference is the substitution of $\boldsymbol{K}_{\text{p-ad-im}}^{(N_1+N_2)}$ for $\boldsymbol{K}_{\text{p-ad-p}}^{(N_1+N_2)}$ in the Eq. (36). And

$$\boldsymbol{K}_{\text{p-ad-im}}^{(N_1+N_2)}=\boldsymbol{K}_{\mathrm{p}}^{(N_1+N_2)}(1\sim 7,1\sim 7) \tag{39}$$

where "im" in the subscript represents the adapted stiffness matrix of the impermeable boundary.

For the interface at $z=z_{N_1+1}$, the same method is used. The upper and lower sides of the interface between the TI elastic and poroelastic layers have the same number of control variables of displacement and stress after handling the element stiffness matrix of TI poroelastic medium of layers N_1+1 and N_1+N_2. Assembly and inversion of total stiffness matrix could be achieved using displacement–stress continuity condition, and the dynamic response is obtained:

$$\boldsymbol{U}=\boldsymbol{K}_{\text{global}}^{-1}\boldsymbol{\Sigma} \tag{40}$$

where $\boldsymbol{K}_{\text{global}}$ is the total stiffness matrix of layered ground; $\boldsymbol{U}$ and $\boldsymbol{\Sigma}$ are the displacement and stress vectors of layered ground. And

$$\boldsymbol{U}=[\hat{\hat{\boldsymbol{u}}}_{\mathrm{e}}(0),\hat{\hat{\boldsymbol{u}}}_{\mathrm{e}}(z_1),\cdots,\hat{\hat{\boldsymbol{u}}}_{\text{e-p}}(z_{N_1}),\hat{\hat{\boldsymbol{u}}}_{\mathrm{p}}(z_{N_1+1}),\cdots,\hat{\hat{\boldsymbol{u}}}_{\text{p-e}}(z_{N_1+N_2}),\cdots,\hat{\hat{\boldsymbol{u}}}_{\mathrm{e}}(z_{N_1+N_2+N_3})]^{\mathrm{T}} \tag{41}$$

$$\boldsymbol{\Sigma}=[\hat{\hat{\boldsymbol{\Sigma}}}_{\mathrm{e}}(0),0,\cdots,0,0,\cdots,0,\cdots,0]^{\mathrm{T}} \tag{42}$$

The subscripts in Eq. (41), "e-p" and "p-e", mean the interface between the TI elastic medium and the TI poroelastic medium, the interface between the TI poroelastic medium and the TI elastic medium, respectively. The superscript "−1" in $\boldsymbol{K}_{\text{global}}$ of Eq. (40) means inverse matrix, also called flexibility matrix.

2.3 Dynamic response of track–TI ground coupled system

In this paper, the track system is simplified as a beam–mass–spring system[3], in which rails and sleepers are simulated with Euler beam elements and mass blocks, respectively, and both are connected using rail pads, where rail pads are simplified as springs without mass. The effect of ballast is simplified as vertical stiffness, and its mass is also considered for simulating the inertial action. Control equations of the above simplified model are shown as follows:

$$EI\frac{\partial^4 u_{\mathrm{r}}}{\partial x^4}+m_{\mathrm{r}}\ddot{u}_{\mathrm{r}}+k_{\mathrm{p}}\left(u_{\mathrm{r}}-u_{\mathrm{s}}\right)=P \tag{43}$$

$$m_{\mathrm{s}}\ddot{u}_{\mathrm{s}}-k_{\mathrm{p}}\left(u_{\mathrm{r}}-u_{\mathrm{s}}\right)=-F_{\mathrm{s}} \tag{44}$$

$$\begin{bmatrix}\dfrac{m_{\mathrm{b}}}{3}\dfrac{\partial^2}{\partial t^2}+k_{\mathrm{b}} & \dfrac{m_{\mathrm{b}}}{6}\dfrac{\partial^2}{\partial t^2}-k_{\mathrm{b}}\\ \dfrac{m_{\mathrm{b}}}{6}\dfrac{\partial^2}{\partial t^2}-k_{\mathrm{b}} & \dfrac{m_{\mathrm{b}}}{3}\dfrac{\partial^2}{\partial t^2}+k_{\mathrm{b}}\end{bmatrix}\begin{Bmatrix}u_{\mathrm{s}}\\ u_{\mathrm{b}}\end{Bmatrix}=\begin{Bmatrix}F_{\mathrm{s}}\\ -F_{\mathrm{b}}\end{Bmatrix} \tag{45}$$

where u_{r}, u_{s} and u_{b} are the vertical displacement of track, sleeper and ballast; EI is the rail bending stiffness; k_{p} and k_{b} are the vertical stiffness of rail pad and ballast; m_{r}、m_{s} and m_{b} are the mass of rail, sleeper and ballast per unit length; P is the loading on the rail per unit length. In this paper, the axle load of the train was simulated as a set of point load, so $P=\sum_{i=1}^{N}P_i\delta(x-ct-a_i)$, where N is the total number of load; P_i and a_i are the i-th load amplitude and the cooridinates at $t=0$ s; δ is the Dirac function; $F_{\mathrm{rs}}=k_{\mathrm{p}}(u_{\mathrm{r}}-u_{\mathrm{s}})$, F_{s} and F_{b} are the forces transmitted from the rail to the sleepers, from the sleepers to the ballast and from the ballast to the ground per unit length.

The boundary conditions on the contact surface of the track and the ground could be set as:

$$\left.\begin{aligned}&\sigma_{xz}^{\mathrm{e}}(x,y,z=0)=0,\ \sigma_{yz}^{\mathrm{e}}(x,y,z=0)=0\\&\sigma_{zz}^{\mathrm{e}}(x,y,z=0)=-\frac{F_{\mathrm{b}}}{2L_{\mathrm{b}}},\ -L_{\mathrm{b}}<y<L_{\mathrm{b}}\\&u_z^{\mathrm{e}}(x,y=0,z=0)=u_{\mathrm{b}}(x)\end{aligned}\right\} \tag{46}$$

where $2L_{\mathrm{b}}$ is the contact width between ballast and ground; σ_{xz}^{e}, σ_{yz}^{e} and σ_{zz}^{e} are the horizontal shear stresses in the x direction and the y direction and the vertical normal stress on the surface; u_z^{e} is the surface displacement; and u_{b} is the displacement of ballast.

Based on Eq.(46), the equivalent flexibility coefficient C for the interaction between the track and the surface of the ground could be derived as

$$C(\xi,\omega)\hat{\bar{F}}_{\mathrm{b}}(\xi,\omega)=\hat{\bar{u}}_{\mathrm{b}}(\xi,\omega) \tag{47}$$

$$C(\xi,\omega)=\frac{1}{2\pi}\int_{-\infty}^{\infty}\hat{\bar{u}}_{z-\mathrm{unit}}^{\mathrm{e}}(\xi,\eta,0,\omega)\frac{\sin(\eta L_{\mathrm{b}})}{\eta L_{\mathrm{b}}}\mathrm{d}\eta \tag{48}$$

where $\hat{\bar{u}}_{z-\mathrm{unit}}^{\mathrm{e}}(\xi,\eta,0,\omega)$ is the dynamic response of the surface vertical displacement obtained by substituting $\hat{\bar{\boldsymbol{\Sigma}}}_{\mathrm{e}}(0)=[0,0,-1]^{\mathrm{T}}$ to Eq. (42).

Fourier transforming Eqs. (43)–(45) with respect to time and space and substituting Eq. (47) into transformed Eq. (45), the stiffness matrix of the track system was derived as follows:

$$\begin{bmatrix}KR_{11} & -k_{\mathrm{p}} & 0\\ -k_{\mathrm{p}} & KR_{22} & -k_{\mathrm{b}}-\dfrac{m_{\mathrm{b}}}{6}\omega^2\\ 0 & -k_{\mathrm{b}}-\dfrac{m_{\mathrm{b}}}{6}\omega^2 & KR_{33}\end{bmatrix}\begin{Bmatrix}\hat{\bar{u}}_{\mathrm{r}}\\ \hat{\bar{u}}_{\mathrm{s}}\\ \hat{\bar{u}}_{\mathrm{b}}\end{Bmatrix}=\begin{Bmatrix}\hat{\bar{P}}\\ 0\\ 0\end{Bmatrix} \tag{49}$$

$$\left.\begin{aligned}KR_{11}&=EI\xi^4-m_{\mathrm{r}}\omega^2+k_{\mathrm{p}}\\KR_{22}&=k_{\mathrm{p}}+k_{\mathrm{b}}-\left(\frac{m_{\mathrm{b}}}{3}+m_{\mathrm{s}}\right)\omega^2\\KR_{33}&=k_{\mathrm{b}}-\frac{m_{\mathrm{b}}}{3}\omega^2+\frac{1}{C(\xi,\omega)}\\\hat{\bar{P}}&=2\pi\delta(\omega-v\xi)\sum_{i=1}^{\mathrm{N}}\left(P_i\mathrm{e}^{\mathrm{i}\xi a_i}\right)\end{aligned}\right\} \tag{50}$$

where $\hat{\bar{P}}$ is the axle load of the train in the transformation domain.

Based on Eq.(49), the value of the dynamic response of the track system in the transformation domain could be obtained, and the final dynamic response could be achieved by conducting inverse Fourier transform:

$$\begin{aligned}u_{\mathrm{b}}(x,t)&=\frac{1}{4\pi^2}\int_{-\infty}^{\infty}\int_{-\infty}^{\infty}\hat{\bar{u}}_{\mathrm{a}}(\xi,\omega)2\pi\delta(\omega-v\xi)\mathrm{e}^{\mathrm{i}\omega t}\mathrm{e}^{-\mathrm{i}\xi x}\mathrm{d}\xi\mathrm{d}\omega=\\&\frac{1}{2\pi v}\int_{-\infty}^{\infty}\hat{\bar{u}}_{\mathrm{a}}(\omega/v,\omega)\mathrm{e}^{\mathrm{i}\omega t}\mathrm{e}^{-\mathrm{i}\omega x/v}\mathrm{d}\omega=\\&\frac{1}{2\pi}\int_{-\infty}^{\infty}\hat{\bar{u}}_{\mathrm{a}}(\xi,v\xi)\mathrm{e}^{\mathrm{i}v\xi t}\mathrm{e}^{-\mathrm{i}\xi x}\mathrm{d}\xi\end{aligned} \tag{51}$$

where $\bar{u}_{\mathrm{a}}$ is the dynamic response under arbitrary loads $\sum_{i=1}^{\mathrm{N}}\left(P_i\mathrm{e}^{\mathrm{i}\xi a_i}\right)$ in the transform domain.

2.4 Verification for solution

In order to verify the solution in this paper, the calculation results of the model were compared with the result of Ba et al.[26]. Ba et al.[26] investigated the dynamic response of the coupled system consisting of the TI elastic layered ground and the track. In this paper, time history curve of ground displacement (Fig. 2) under the single axle load was obtained by using the same parameters with Ba et al. [26], and in calculation, $v=1.8c^*$, $E_{\mathrm{h}}/E_{\mathrm{v}}=2$, and $x/B=0$ m (v is the load velocity and c^* is the reference velocity, and the definitions of them could be found in Ba et al.[26]). According to Fig.2, the calculation result using the method proposed in this paper is consistent with that of Ba et al.[26], and the solution was verified.

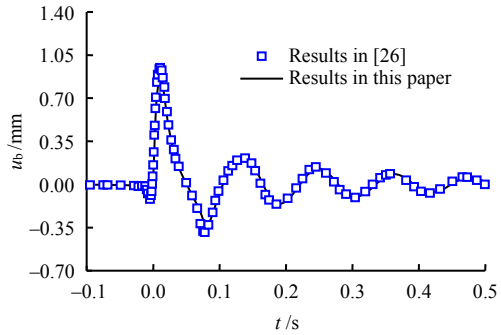

Fig. 2 Solution verification

3 Dynamic response of track–TI ground under the single axle load

In this section, the dynamic response of the system will be discused, and the influences of the existence of groundwater and the stiffness of the underlying TI elastic half-space on the dynamic response are analyzed. Unless otherwise specified, $N_1=1$, $N_2=1$ and $N_3=0$ in the model in Fig. 1 are selected for example analysis.

The parameters of the track are as follows[3]: $EI=1.26\times10^7$ Pa·m^2; $k_p=3.5\times10^8$ Pa; $k_b=3.15\times10^8$ Pa, the corresponding damping are $\eta_p=0.15$ and $\eta_b=1$; the mass per unit length are $m_r=120$ kg/m, $m_s=490$ kg/m and $m_b=1\ 200$ kg/m; a half width of the contact area between the ballast and the ground is $L_b=1.35$ m. The values of parameters of the ground are in the range of commonly used those in the papers[1, 3, 9, 11, 23, 26], and these values selected are as follows: For the 1st TI elastic layer, $\rho^e=1\ 800$ kg/m^3, $E_h^e=1.44\times10^8$ Pa, $E_v^e=8\times10^7$ Pa, $G_v^e=3\times10^7$ Pa, $h_1=4$ m (h_1 is the thickness of the 1st layer), $\nu_v^e=\nu_{vh}^e=0.33$. For the 2nd TI poroelastic layer, $\rho_f=1\ 000$ kg/m^3, $\rho_s=2\ 650$ kg/m^3, $n=0.388$, $E_h=4.5\times10^7$ Pa, $E_v=2.5\times10^7$ Pa, $G_v=9.4\times10^6$ Pa, $\nu_h=\nu_{vh}=0.33$, $a_{\infty1}=a_{\infty3}=1.789$, $K_s=3.65\times10^{10}$ Pa, $K_f=2.25\times10^9$ Pa, $\eta_f=10^{-3}$ Pa·s, $k_1=k_3=10^{-11}$ m^2, $h_2=8$ m. For TI half-space, $\rho^e=2\ 100$ kg/m^3, $E_h^e=2.7\times10^9$ Pa, $E_v^e=1.5\times10^9$ Pa, $G_v^e=6\times10^8$ Pa, $\nu_v^e=\nu_{vh}^e=0.25$.

Various media were utilized to simulate the soil layers with various water content conditions in the model in this paper. In TI poroelastic layer, the groundwater table was considered. In order to analyze the influence of groundwater on the dynamic response, the dynamic amplification factor of the track model system in this paper was compared with that of the equivalent layered TI elastic ground–track coupled model, as shown in Fig. 3. In the equivalent layered TI elastic ground model, the TI poroelastic layer in the model proposed in this paper was replaced as the the equivalent layered TI elastic layer, and the density of the elastic layer is $\rho^e=n\rho_f+(1-n)\rho_s$, in which the elastic parameters are the same as those of the model in this paper. In Fig.3, P_m/P_0 is the amplification factor. P_0 is the amplitude of the load on the rail; P_m ($m=$ rs, s, b) is the amplitude of the integral of F_m in the x direction, and its definition is as follows:

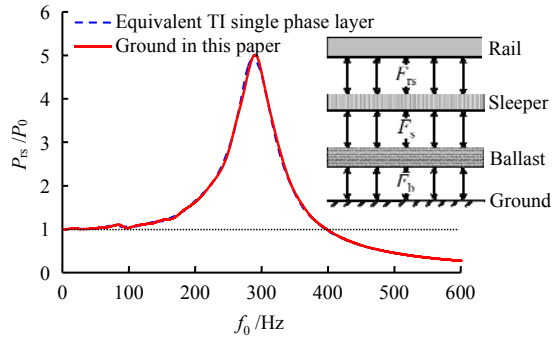

(a) P_{rs}/P_0-f_0 curves

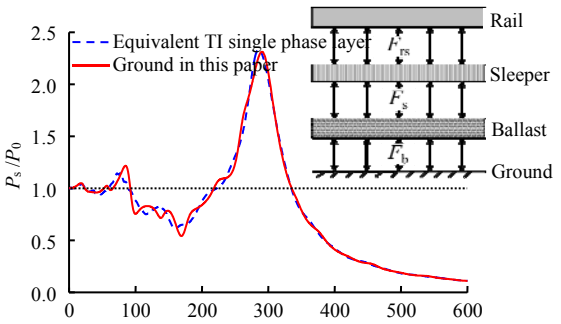

(b) P_s/P_0-f_0 curves

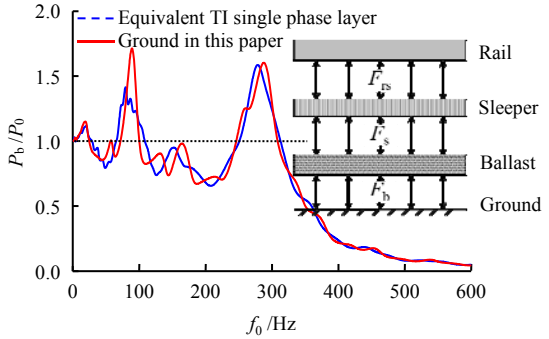

(c) P_b/P_0-f_0 curves

Fig. 3 Influences of groundwater existence on force amplification factor of track system

$$P_m=\left|\int_{-\infty}^{\infty}F_m(x,2\pi f_0)\mathrm{d}x\right|=\left|\hat{F}_m(\xi=0,2\pi f_0)\right| \quad (52)$$

where f_0 is the load frequency; m=rs, s, b mean P_m represent the coefficients of rail–sleeper, sleeper–allast and ballast–ground, respectively.

The amplification coefficients of the force between rails and sleepers are shown in Fig. 3(a). The results based on two models are approximately consistent with each other, and the difference is at the peak of curves. This could be attributed to the same parameters of two models and the small influence of groundwater because of the large distance between the contact area of rail–sleeper and the ground. When $f_0<100$ Hz, $P_{rs}/P_0\approx1$. The value of P_{rs}/P_0 reaches the peak value of approximately 5, at $f_0=289$ Hz, which is the resonance frequency and is close to the natural frequency of the ideal rail–spring system, $f_r=\sqrt{k_p/m_r}/(2\pi)=272$ Hz. Figures 3(b) and 3(c) are the amplification coefficients of the force of sleeper–ballast and the ballast–ground, respectively. The influence of groundwater increases

with decreasing the distance between the monitoring locations and the ground, and the influence on P_b / P_0 is the most. The influence of groundwater is obvious in the range of low frequency $f_0 < 200$ Hz, while in the range of relative high frequency, the curves according to two models are consistent. This could be attributed to the drainage conditions. In the low frequency range, the water of the TI poroelastic layer in the model of this paper could be fully drained, and there is a larger relative displacement between the solid and the liquid. However, in the equivalent model, the relative displacement cannot occur. And this difference leads to the different results. In the high frequency range, there is a smaller relative displacement between the solid and the liquid due to no time to drain the pore water. Thus, the TI poroelastic layer is similar to an undrained layer, and its property is close to the equivalent TI elastic layer and the curves of the two models are almost consistent with each other. For the track–ground system in this paper, the maximum values of P_s / P_0 and P_b / P_0 are 2.3 and 1.7, respectively.

The influence of the stiffness of the half-space of TI elastic medium on the dynamic response of the system is shown in Fig. 4, and the model proposed by this paper is also compared with the model considering the overlying TI elastic layer and poroelastic layer and the underlying rigid layer in this figure. The surface displacement distributions in the x direction at $y = 30$ m in three different vertical elastic modulus cases, such as $E_v^e = 1.5\times10^8$ Pa, $E_v^e = 1.5\times10^9$ Pa and rigid layer, are shown in Fig. 4. In these three cases, the parameters of 1st layer and 2nd layer are the same, and the velocity of load is $0.8\,v_0$. Without special instructions, hereafter the definition of reference velocity is $v_0 = \sqrt{G_0 / \rho_0} = 129$ m/s, and G_0 and ρ_0 are the shear modulus and the density of 1st layer, respectively. As we can see, in the case of $E_v^e = 1.5\times10^8$ Pa, the surface vibration is stronger than that in the case of $E_v^e = 1.5\times10^9$ Pa. And the results of $E_v^e = 1.5\times10^9$ Pa are close to those of the rigid layer model. For quantification of the difference of the dynamic response in the different stiffness cases of half-space, the definition of the relative value R_{uz} of difference is as follows:

$$R_{uz} = \frac{|u_{z|2}(x) - u_{z|1}(x)|}{\max\left(|u_{z|1}(x)|\right)} \tag{53}$$

where $u_{z|2}$ is the displacement of the half-space with $E_v^e = 1.5\times10^8$ Pa or the rigid layer; $u_{z|1}$ is the displacement response of the the half-space with $E_v^e = 1.5\times10^9$ Pa, and this value was selected as the reference value. As we can see, the maximum difference between the displacement response of the half-space of $E_v^e = 1.5\times10^8$ Pa and the reference value is 78.0 %, and for the rigid layer, this maximum difference is 6.3%. Thus, the stiffness of the half-space has a relatively large influence on the surface displacement. Compared with the model of the rigid layer, the model in this paper could simulate the layer with various stiffness, and could consider the stress distribution in the half-space.

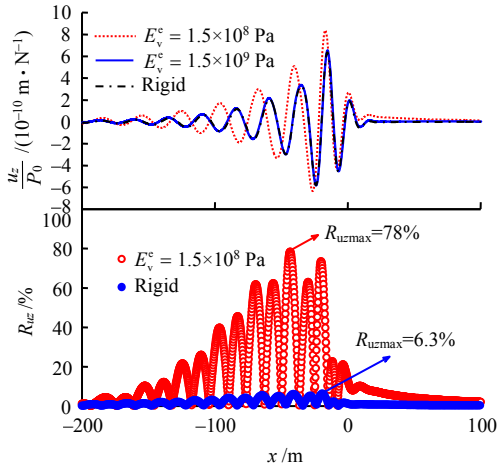

Fig. 4 Influences of stiffness of underlying half-space on displacement

4 Dynamic response of track–round under multi axial loads

This section studies the dynamic response of the track–TI ground under multi axial loads with different transversely isotropic conditions. Based on the previous studies[23], the transverse isotropy of the ground is mainly characterized by the ratio of horizontal and vertical elastic modulii (E_h / E_v).

The amplitude of axle loads and the coordinates at $t = 0$ s are listed in Table 1[31].

Table 1 Parameters of axle loads

No.	a_i /m	P_i /kN	No.	a_i /m	P_i /kN
1	−58.785	181.5	11	0.000	122.5
2	−55.885	181.5	12	2.900	122.5
3	−49.285	180.0	13	6.700	122.5
4	−46.385	180.0	14	9.600	122.5
5	−42.100	122.5	15	24.400	122.5
6	−39.200	122.5	16	27.300	122.5
7	−24.400	122.5	17	29.585	122.5
8	−21.500	122.5	18	32.485	122.5
9	−17.700	122.5	19	44.085	122.5
10	−14.800	122.5	20	46.985	122.5

Considering the value of E_h / E_v of three different TI grounds, E_h of each layer of these three conditions are:(i) $E_{h|1}^e = 1.44\times10^8$ Pa, $E_{h|2} = 4.5\times10^7$ Pa, $E_{h|3}^e = 2.7\times10^9$ Pa; (ii) $E_{h|1}^e = 8\times10^7$ Pa, $E_{h|2} = 2.5\times10^7$ Pa, $E_{h|3}^e = 1.5\times10^9$ Pa; (iii) $E_{h|1}^e = 4.4\times10^7$ Pa, $E_{h|2} = 1.375\times10^7$ Pa, $E_{h|3}^e = 8.25\times10^8$ Pa. 1, 2 and 3 in the subscript represent the number of layers, and 1, 2 and 3 represent 1st layer, 2nd layer and the underlyinghalf-space, respectively. In (i)–(iii), the values of E_v and other parameters in each layer are the same as those in section 3. The three cases, (i)–(iii), represent $(E_h / E_v)_i < 1$, $(E_h / E_v)_i = 1$ and $(E_h / E_v)_i > 1$, respectively; i=1, 2, 3 are the number of layers, and $(E_h / E_v)_i < 1$ means the values of E_h / E_v are all smaller than 1 in the three layers of the ground.

Figure 5 shows the variation of the maximum rail displacement with the dimensionless velocity under

different transversely isotropic conditions. It can be found that there is a peak value in the rail displacement curve, and the velocity corresponding to the peak value is the critical velocity of the dynamic response. The critical velocity phenomenon is the resonance phenomenon caused by the load velocity reaching the surface wave phase velocity of the track–ground system. With the increase of $(E_h / E_v)_i$, the amplitude of dynamic response decreases gradually, and the corresponding critical velocity increases from $0.65\,v_0$ to $0.7\,v_0$ and $0.81\,v_0$.

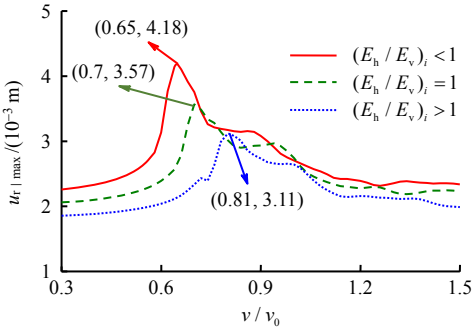

Fig. 5 Variations of the maximum displacement of rail with load speed

The relationship between the maximum vertical displacement and the load velocity at $y = 20$ m on the surface is plotted in Fig. 6 under different transversely isotropic conditions. By comparing with Fig. 5, it can be found that the critical velocity of vertical displacement at $y = 20$ m is consistent with that of the rail, and the variation of response amplitude with $(E_h / E_v)_i$ is the same. However, when the load speed is less than a certain value ($0.52\,v_0$, $0.58\,v_0$, $0.66\,v_0$), the displacement amplitude is almost zero, and then the dynamic response continues to rise. This speed is called cut-off speed[32]. When the load velocity is less than the cut-off speed, the surface response is quasi-static, and there is no wave propagation in the ground.

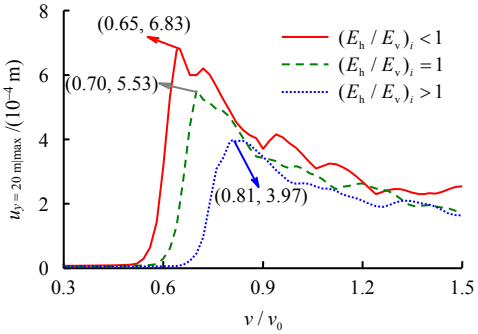

Fig. 6 Variations of the maximum displacement of ground surface at *y*=20 m with load speed

Figure 7 shows the attenuation of surface displacement with the distance from the track center under different transversely isotropic conditions. The displacement amplitude is represented by the dimensionless quantity VUL, and the unit is dB. $\mathrm{VUL} = 20\lg(u_z / u_{re})$, and $u_{re} = 10^{-12}$ m. The rate of displacement attenuation is the slowest when $(E_h / E_v)_i < 1$, and the attenuation of dynamic response is the fastest when $(E_h / E_v)_i > 1$. And it can be seen that when $(E_h / E_v)_i < 1$, the VUL curve fluctuates with the distance y, and there is a phenomenon of amplification region (the VUL increases locally). This phenomenon could be attributed to the superposition of surface Rayleigh wave and the interlayer interface reflection wave. However, when $(E_h / E_v)_i > 1$, the curve has no obvious fluctuation, which may be due to the change of soil layer property, resulting in the decrease of reflectivity of wave at the interface between layers, thereby no obvious superposition of waves on the surface.

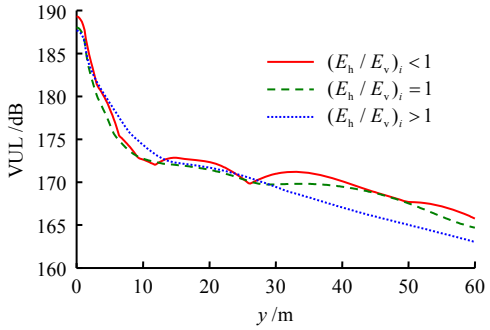

Fig. 7 Variations of VUL with *y*

The displacement response spectrum every 10 m at $y = 0$–60 m is shown in Fig. 8. The broken line 1 connects the spectrum peaks of each region, the broken line 3 connects the upper limit value of each region, and the broken line 2 is the spectrum at different locations.

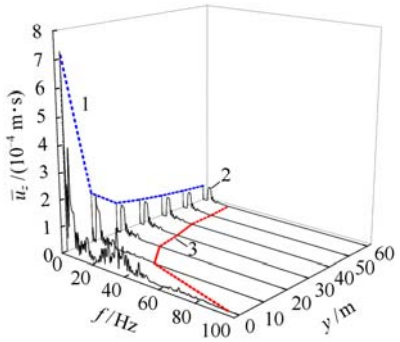

(a) $(E_h / E_v)_i < 1$

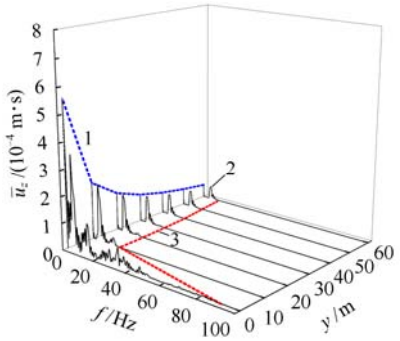

(b) $(E_h / E_v)_i > 1$

Fig. 8 Fourier spectrum of surface displacement at different locations

The attenuation of amplitude and distribution width are obvious in the range of $y=0$–10 m. In the range of 20–60 m, the attenuation is slow, and in the range of $y>30$ m, the frequency spectrum only includes the part smaller than 20 Hz for both the two values of $(E_h/E_v)_i$. As we can see from the comparison of Figs. 8(a) and 8(b), at $y=0$ m, both the displacement amplitudes of the two transversely isotropic conditions are in the range of 0–94 Hz, and mainly concentrated in 0–50 Hz. At $y=10$ m, the corresponding displacement amplitudes of $(E_h/E_v)_i<1$ and $(E_h/E_v)_i>1$ are attenuated to the ranges of 0–40 Hz and 0–18 Hz, respectively. With the increase of y, the spectrum distribution range of $(E_h/E_v)_i>1$ are smaller than that of $(E_h/E_v)_i<1$.

The minimum value distributions of vertical stress $\sigma_{zz|\min}$, at $x=0$ m, $y=0$ m (the maximum amplitude and negative compression stress) under different transversely isotropic conditions are depicted in Fig.9. The dashed lines in the figure are the interfaces between layers. The peaks $\sigma_{zz|\min}$ occur in the range of 0.0–1.0 m away from the surface, and they would decrease with the increase of $(E_h/E_v)_i$. The peak positions are 0.60, 0.36 and 0.28 m for $(E_h/E_v)_i<1$, $(E_h/E_v)_i=1$ and $(E_h/E_v)_i>1$, respectively. In 1st layer (TI elastic layer), $|\sigma_{zz|\min}|$ is the smallest when $(E_h/E_v)_i>1$, while in 2nd layer as well as the half-space, $|\sigma_{zz|\min}|$ is the largest when $(E_h/E_v)_i>1$. This phenomenon could be explained by combining with the local increase of the displacement response (see Fig.7). When $(E_h/E_v)_i<1$, the reflected wave energy of the interface between the 1st layer and the 2nd layer is large, and the vibration is mainly concentrated in the 1st layer. However, when $(E_h/E_v)_i>1$, the reflection wave energy of the interface between 1st layer and 2nd layer is smaller, and the transmission wave energy entering 2nd layer and the half-space is larger, so the stress amplitude is larger in 2nd layer and the half-space. Moreover, it can be found that there is still stress distribution in the TI elastichalf-space, and this situation can further indicate that the analysis of the complete rigid base model in Fig.4 will lead to errors.

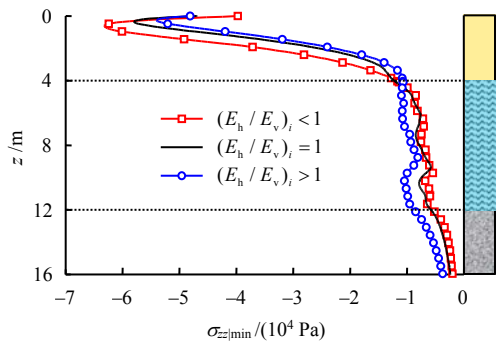

Fig. 9 Distribution of $\sigma_{zz|\min}$ with depth at x=0 m, y=0 m

Under the different transversely isotropic conditions, the variation of $\sigma_{zz|\min}$ with the velocity of load at z = 1, 10, 14m is presented in Fig. 10. There are velocity peaks, and their values are higher than the critical velocities in Figs. 5 and 6. At different depths, the peak velocity is increasing with increasing $(E_h/E_v)_i$, and the variation rule is consistent with the rule of surface displacement critical velocity with $(E_h/E_v)_i$. However, at $z=10$ m and 14 m, the peaks of $\sigma_{zz|\min}$ are increaseing with increasing $(E_h/E_v)_i$, and the trends are opposite with that of displacement Figs. 5 and 6.

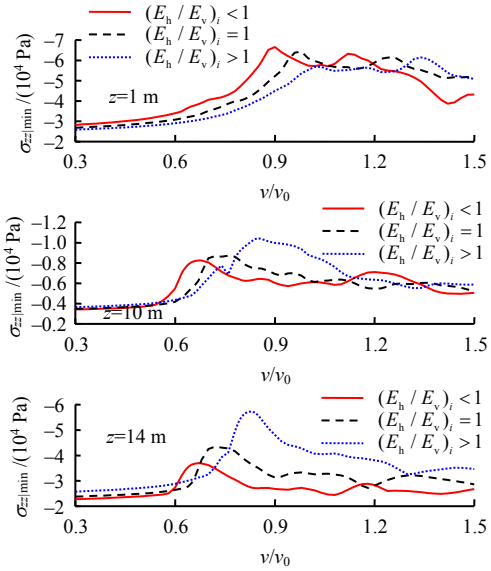

Fig. 10 Variations of $\sigma_{zz|\min}$ with load speed at different depths

Under different transversely isotropic conditions, the excess pore pressure distributions in TI poroelastic layers are illustrated in Fig. 11. The phenomenon of "Mach cone" exists when the positive pore pressure is generated under the axial load and its distribution is inclined along with the depth. The excess pore pressure with $(E_h/E_v)_i>1$ is larger than that with $(E_h/E_v)_i<1$. And when $(E_h/E_v)_i<1$, excess pore pressure is mainly concentrated on the upper interface of TI poroelastic layer, while when $(E_h/E_v)_i>1$, the distribution of excess pore pressure is more uniform along with the depth.

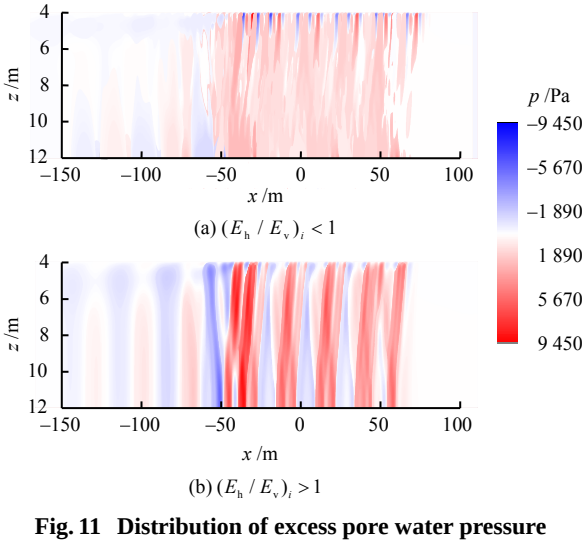

Fig. 11 Distribution of excess pore water pressure

5 Conclusion

To study the environmental vibration caused by train operation, an analytical model of coupled ground–track considering the alternating distribution of elastic and poroelastic TI layers is established. Compared with the existing track–elastic medium foundation model, the proposed model simulates TI soil layers with different water content conditions in the ground, taking into account the influences of groundwater level and underlying ground. To investigate the dynamic response of track–ground coupled system, the governing equations of TI medium are solved based on Fourier transform and potential function method; then, the exact stiffness matrix method is adapted to derive the solution of multi-layer foundation with different TI media; after that, the analytical solution of the dynamic response in the transform domain is obtained by coupling the track and ground; finally, the inverse transform is used to gain the dynamic response in time and space domain, and the influences of the existence of groundwater, the stiffness of underlying layer and transverse isotropy on the vibration propagation law are analyzed.

(1) The influence of groundwater in TI poroelastic layer on the load amplification factor of the track system is obvious when the load frequency is lower than 200 Hz. The maximum amplification factors of the forces of rail–sleeper, sleeper–ballast and ballast– round are 5.0, 2.3 and 1.7, respectively. Compared with the rigid base model, the TI half-space in this model can simulate the base with arbitrary stiffness and the wave propagation in the base.

(2) The attenuation speed of the surface vibration along with the direction perpendicular to the track increases with the increase of the transversely isotropic parameters $(E_{\mathrm{h}}/E_{\mathrm{v}})_i$, and there is a phenomenon of amplification under condition of $(E_{\mathrm{h}}/E_{\mathrm{v}})_i<1$, which is generated by the superposition of the interlayer reflection wave and the surface Rayleigh wave. The spectrum of surface displacement decays to 20 Hz when the distance larger than 30 m

(3) The maximum vertical stress is in the range of 1.0 m away from the surface, and the location of this value is decreasing with increasing $(E_{\mathrm{h}}/E_{\mathrm{v}})_i$. In the 1st layer, the amplitude of vertical stress is the maximum when $(E_{\mathrm{h}}/E_{\mathrm{v}})_i<1$, whilst in the 2nd layer and the half-space, the amplitude of vertical stress is the maximum when $(E_{\mathrm{h}}/E_{\mathrm{v}})_i>1$. This could be attributed to that the energy ratio of the reflected wave and the transmitted wave is changed by the change of the $(E_{\mathrm{h}}/E_{\mathrm{v}})_i$.

(4) The critical velocity and amplitude of the vertical displacement of the track and the ground surface increase and decrease with the increase of the transversely isotropic coefficient, respectively. The critical velocity and amplitude of the vertical stress in the 2nd layer and the half-space are positively correlated with $(E_{\mathrm{h}}/E_{\mathrm{v}})_i$. When $(E_{\mathrm{h}}/E_{\mathrm{v}})_i<1$, the excess pore pressure is concentrated near the upper boundary, while when $(E_{\mathrm{h}}/E_{\mathrm{v}})_i>1$, the excess pore pressure is mainly distributed in the whole TI poroelastic layer depth.

Referneces

[1] BA Zhen-ning, LIANG Jian-wen, JIN Wei. Dynamic response of coupled system of track and layered fluid-saturated ground under moving high-speed loads[J]. Engineering Mechanics, 2015, 32(11): 189–200.

[2] DIETERMAN H A, METRIKINE A. The equivalent stiffness of a half-space interacting with a beam: critical velocities of a moving load along the beam[J]. European Journal of Mechanics－A/Solids, 1996, 15(1): 67–90.

[3] SHENG X, JONES C J C, PETYT M. Ground vibration generated by a harmonic load acting on a railway track[J]. Journal of Sound & Vibration, 1999, 225(1): 3–28.

[4] JONES C J C, SHENG X, PETYT M. Simulations of ground vibration from a moving harmonic load on a railway track[J]. Journal of Sound and Vibration, 2000, 231(3): 739–751.

[5] FENG Qing-song, LEI Xiao-yan, LIAN Song-liang. Vibration analysis of high-speed railway subgrade-ground system[J]. Journal of Railway Science and Engineering, 2010, 7(1): 4–9.

[6] HUANG Qiang, LIU Gan-bin, LÜ Qing, et al. Comparative analysis of dynamic responses of Timoshenko beams on visco-elastic foundations under moving loads[J]. Applied Mathematics and Mechanics, 2020, 41(7): 735–746.

[7] BIOT M. Theory of propagation of elastic waves in a fluid-saturated porous solid. I. low-frequency range[J]. The Journal of the Acoustical Society of America, 1956, 28(2): 168–178.

[8] JIN B. Dynamic displacements of an infinite beam on a poroelastic half space due to a moving oscillating load[J]. Archive of Applied Mechanics, 2004, 74(3/4): 277–287.

[9] XU B, LU J F, WANG J H. Dynamic response of an infinite beam overlying a layered poroelastic half-space to moving loads[J]. Journal of Sound & Vibration, 2007, 306(1–2): 91–110.

[10] CAI Y, SUN H, XU C. Response of railway track system on poroelastic half-space soil medium subjected to a moving train load[J]. International Journal of Solids and Structures, 2008, 45(18): 5015–5034.

[11] CAO Z, BOSTRÖM A. Dynamic response of a poroelastic half-space to accelerating or decelerating trains[J]. Journal of Sound & Vibration, 2013, 332(11): 2777–2794.

[12] YAO H L, HU Z, LU Z, et al. Analytical model to predict dynamic responses of railway subgrade due to high-speed

trains considering wheel-track interaction[J]. International Journal of Geomechanics, 2016, 16(2): 04015061.

[13] BARDEN L. Stresses and displacements in a cross-anisotropic soil[J]. Geotechnique, 1963, 13(3): 198–210.

[14] LI Guang-xin. Advanced soil mechanics[M]. Beijing: Tsinghua University Press, 2004.

[15] TIAN Yu, YAO Yang-ping, LU De-chun, et al. Cross-anisotropic Mohr-Coulomb criterion and formula of passive earth pressure based on modified stress method[J]. Rock and Soil Mechanics, 2019, 40(10): 3945–3950.

[16] HU Hai-chang. On the vibration of a transversely isotropic elastic body[J]. Acta Physica Sinica, 1955, 11(3): 231–238.

[17] ESKANDARI-GHADI M, PAK R Y S, ARDESHIR-BEHRESTAGHI A. Transversely isotropic elastodynamic solution of a finite layer on an infinite subgrade under surface loads[J]. Soil Dynamics and Earthquake Engineering, 2008, 28(12): 986–1003.

[18] HAN Ze-jun, LIN Gao, ZHOU Xiao-wen, et al. Solution and analysis of dynamic stress response for transversely isotropic multilayered soil[J]. Rock and Soil Mechanics, 2018, 39(6): 2287–2294.

[19] YAN Ke-zhen, MAN Jian-hong, SHI Ting-wei, et al. Analytical solution for dynamic response of transversely isotropic structures considering the state of interlayer contact state[J]. Journal of Hunan University (Natural Science), 2019, 46(11): 97–105.

[20] AI Z, MU J, REN G. 3D dynamic response of a transversely isotropic multilayered medium subjected to a moving load[J]. International Journal for Numerical and Analytical Methods in Geomechanics, 2018, 42(4): 636–654.

[21] BA Zhen-ning, ZHOU Xu, LIANG Jian-wen. Scattering of plane qP-qSV waves by a convex topography based on the transversely isotropic medium[J]. Rock and Soil Mechanics, 2019, 40(1): 379–387.

[22] WANG Xiao-gang. Dynamic Green's function for internal barrel loads in transversely isotropic saturated soils[J]. Chinese Journal of Theoretical and Applied Mechanics, 2010, 42(5): 909–918.

[23] BA Z N, LIANG J W. Fundamental solutions of a multi-layered transversely isotropic saturated half-space subjected to moving point forces and pore pressure[J]. Engineering Analysis with Boundary Elements, 2017, 76: 40–58.

[24] SAHEBKAR K, ESKANDARI-GHADI M. Dynamic behaviour of an infinite saturated transversely isotropic porous media under fluid-phase excitation[J]. Soil Dynamics and Earthquake Engineering, 2018, 107: 390–406.

[25] LU Jian-fei, ZHOU Hui-ming, LIU Yang. Reflection-transmission matrix method for dynamic response of transversely isotropic multilayered saturated soil[J]. Rock and Soil Mechanics, 2018, 39(6): 2219–2226.

[26] BA Z N, LIANG J W, LEE V W, et al. A semi-analytical method for vibrations of a layered transversely isotropic ground-track system due to moving train loads[J]. Soil Dynamics and Earthquake Engineering, 2019, 121: 25–39.

[27] ZHOU Ye, ZHENG Rong-yue, LIU Gan-bin. Dynamic response of elastic layer on transversely isotropic saturated soil to train load[J]. Rock and Soil Mechanics, 2011, 32(2): 604–610.

[28] ZHAN Y X, YAO H L, LU Z, et al. Dynamic analysis of slab track on multi-layered transversely isotropic saturated soils subjected to train loads[J]. Earthquake Engineering and Engineering Vibration, 2014, 13(4): 731–740.

[29] LI Y C, FENG S J, CHEN H X, et al. Dynamic response of a stratified transversely isotropic half-space with a poroelastic interlayer due to a buried moving source[J]. Applied Mathematical Modelling, 2020, 82: 45–71.

[30] CHAHOUR K, LEFEUVE-MESGOUEZ G, MESGOUEZ A. Spectral analysis of a railway track in contact with a multilayered poroviscoelastic soil subjected to a harmonic moving load[J]. Soil Dynamics and Earthquake Engineering, 2014, 64: 24–37.

[31] TAKEMIYA H. Simulation of track-ground vibrations due to a high-speed train: the case of X-2000 at Ledsgard[J]. Journal of Sound and Vibration, 2003, 261(3): 503–526.

[32] MADSHUS C, KAYNIA A M. High-speed railway lines on soft ground: dynamic behaviour at critical train speed[J]. Journal of Sound and Vibration, 2000, 231(3): 689–701.